Modeling and optimization of nonylphenol removal from contaminated water media using a magnetic recoverable composite by artificial neural networks

Javad Salimi, Babak Kakavandi, Ali Akbar Babaei, Afshin Takdastan, Nadali Alavi, Abdolkazem Neisi and Baharak Ayoubi-Feiz

ABSTRACT

Herein, activated carbon impregnated iron oxide nanoparticles (Fe_3O_4/AC) were synthesized to determine their potentials for the adsorption of nonylphenol (NP) in aqueous solution with different experimental variables, namely the pH of the solution, contact time, adsorbent dosage and the initial NP concentration. Additionally, an artificial neural network system was used to find the relative importance of each of the aforementioned input variables on NP adsorption efficiency. Experimental findings indicated that the optimum solution pH for NP adsorption was 3.0. The equilibrium time of the adsorption process was 30 min. According to the results of isotherm and kinetic studies, among all applied models, the Liu and pseudo-first-order models showed the best fit with the experimental data. The pH of the solution, compared to other input variables, had the maximum impacts on NP adsorption efficiency. Under optimum conditions, the adsorption percentage decreased insignificantly from 99.6 to 92.6% after the fifth cycle. Also, the adsorption efficiencies of 70.7, 73.5 and 67.3% were observed for river water, tap water and wastewater effluent, respectively. Ultimately, from the findings of this study, it can be postulated that Fe_3O_4/AC nanoparticles can be recommended as a promising and novel adsorbent to remove NP from polluted groundwater.

Key words | adsorption, aqueous solution, artificial neural networks, nonylphenol, optimization

Javad Salimi
Babak Kakavandi
Ali Akbar Babaei (corresponding author)
Afshin Takdastan
Abdolkazem Neisi
Environmental Technologies Research Center,
Ahvaz Jundishapur University of Medical Sciences,
Ahvaz, Iran
E-mail: *babaei-a@ajums.ac.ir*

Javad Salimi
Department of Environmental Health Engineering,
School of Health, Torbat Heydariyeh University of Medical Sciences,
Torbat Heydariyeh, Iran

Babak Kakavandi
Student Research Committee,
Ahvaz Jundishapur University of Medical Sciences,
Ahvaz, Iran

Javad Salimi
Ali Akbar Babaei
Afshin Takdastan
Abdolkazem Neisi
Department of Environmental Health Engineering, School of Public Health,
Ahvaz Jundishapur University of Medical Sciences,
Ahvaz, Iran

Nadali Alavi
Environmental and Occupational Hazards Control Research Center,
Shahid Beheshti University of Medical Sciences,
Tehran, Iran
and
Department of Environmental Health Engineering, School of Public Health,
Shahid Beheshti University of Medical Sciences,
Tehran, Iran

Baharak Ayoubi-Feiz
Department of Applied Chemistry, Faculty of Chemistry,
University of Tabriz,
Tabriz, Iran

INTRODUCTION

In the past few decades, rapid development of industrialization has triggered environmental pollution by various contaminants. Among all hazardous organic pollutants, nonylphenol (NP) is intrinsically a xenophobic substance from an organic compound family known as alkylphenols. NP is used in the manufacture of various materials such as laundry and dish detergents, emulsifiers, solubilizers, and antioxidants (USEPA 1996). However, the major reason for the presence of NP in the water and soil resources is the decomposition and degradation of nonylphenolethoxylates (Birkett & Lester 2002). The typical concentrations of NP in river water, landfill leachates and drinking water have been reported in the ranges 0.7 ng/L to 1.5 μg/L (Bester *et al.* 2001), 10–170 μg/L (Öman & Hynning 1993) and 15–85 μg/L

doi: 10.2166/wst.2016.523

(Petrovic *et al.* 2003), respectively. Despite the extremely low concentration of NP in aquatic environments, it can result in massive toxicity in marine creatures.

Up to now, a wide range of remediation techniques such as photochemical oxidation (Fonseca *et al.* 2004; Ide *et al.* 2011), electrochemical decomposition (Kuramitz *et al.* 2002), and biodegradation (Armenante *et al.* 1999) have been applied to remove NP from the environment but their financial and operational difficulties have made researchers hesitant to employ them in a large scale. Therefore, the application of a promising, innovative, and economical approach seems to be a vital necessity. Adsorption is known as one of the most desirable processes to control the excessive concentrations of such pollutants. Hence, different conventional adsorbents (e.g. activated carbon (Jafari *et al.* 2016), carbon nanotube (Shirmardi *et al.* 2013), sediments (Liping *et al.* 2014) and spent tea (Babaei *et al.* 2015)) have so far been used for the adsorption of various contaminants. Of these applied adsorbents, activated carbon has been more welcomed by environmentalists compared with other adsorbents for its cost-effectiveness feature, a high porosity in structure, and a large capacity to adsorb a wide spectrum of contaminants (Asgari *et al.* 2013; Kakavandi *et al.* 2016a). Although these adsorbents have a high adsorption capacity, specifically in low concentrations of contaminants, their difficult application in process engineering due to their small particle size, dispersion in the medium, and separation and filtration problems has obliged researchers to synthesize the magnetic adsorbents.

In general, findings of previous studies have shown that iron particles, either in micro or nano sizes, have an undeniable role in treatment of contaminated aqueous media (Liu *et al.* 2015; Xing *et al.* 2016). In addition to their high tendency towards reacting with a wide range of contaminants, their magnetic features enable them to be separated from aqueous solution using a strong magnetic field (Esfahani *et al.* 2014a). On the other hand, powder activated carbon (PAC) triggers several problems in site remediation due to its high dispersivity and tiny particle size. Therefore, combining both PAC and iron magnetic nanoparticles will not only provide better kinetics for the adsorption of contaminants, but also prevent the aforementioned operational problems and secondary pollution (Mohseni-Bandpi *et al.* 2015; Kakavandi *et al.* 2016b).

The conventional methods of examining batch experiments include studying the impacts of a factor by keeping the other effective experimental agents constant. Obviously, this approach suffers from a lack of possibility to find the interaction effects of input variables. It also increases the costs of operation by the need for a large number of experiments. Such restrictions can be decreased by means of applying an optimization approach that covers not only the interaction effects of input variables but their individual impacts as well. Among all optimization techniques, artificial neural networks (ANNs) constitute one of the most well-known and authenticated methods, which have been used for optimizing a wide range of remediation processes such as reduction, adsorption, Fenton oxidation (Kakavandi *et al.* 2016c), and photocatalytic degradation (Khataee *et al.* 2010). The ANN is intrinsically a progressive mathematical method which draws the output according to the experimental conditions. In addition, it was widely applied to model the rate of removal in the adsorption of contaminants in a solid–liquid system (Balci *et al.* 2011). A brilliant study in this regard would be that of Khataee and co-workers (Hassani *et al.* 2014) in which they predicted the effects of each experimental variable on the adsorption efficiency of a cationic dye on Turkish lignite by means of neural network modeling.

Although the ANN approach was applied to optimize the removal of various contaminants from an aqueous solution, its efficiency for the modeling of NP removal using Fe_3O_4/AC nanoparticles has not been discussed fully. Therefore, the aims of this study are the optimization of NP removal using Fe_3O_4/AC as well as finding the effects of each input variable. Furthermore, the best kinetic and isotherm models for NP adsorption are introduced. The adsorption thermodynamics and reusability of the Fe_3O_4/AC nanoparticles are also studied. Finally, the potential of the composite for removal of NP in real water is evaluated.

MATERIALS AND METHODS

Chemicals

Stock solution of NP was prepared by dissolving a suitable amount of NP in a specific volume of methanol. NP was obtained from Sigma Aldrich Co. while concentrated hydrochloric acid (12 N HCl), sodium hydroxide (NaOH), acid nitric (HNO_3, 65%), PAC and ferric nitrate ($Fe(NO_3)_3.9H_2O$) were purchased from Merck, Darmstadt, Germany. All reagents were analytical grade.

The synthesis and characterization of Fe_3O_4/AC nanoparticles

The synthesis of Fe_3O_4/AC nanoparticles was performed based on the Kakavandi *et al.* (2015) method. Accordingly, at the first stage and in order to homogenize the solution,

specific amounts of activated carbon powder were saturated in 65% nitric acid and then put into an ultrasonic bath for around 3 hours at 80 °C. Afterwards, the filtered carbon was mixed with 200 mL of ferric solution and then placed into an ultrasonic bath for 1 hour. After the filtration of obtained powder, it was kept in an electric oven at 80 °C under N_2 gas for 3 hours. Finally, the synthesized composite was washed sequentially using distilled water in close proximity of a magnetic field and then dried at 105 °C in an oven and kept in a desiccator overnight. The schematic diagram of different steps of the synthesis of Fe_3O_4/AC nanoparticles is given in Figure 1.

The structure and surface characteristics of AC and Fe_3O_4/AC nanoparticles and size of Fe_3O_4 particles were evaluated with a scanning electron microscope (SEM, Philips XL30) and transmission electron microscope (TEM, Philips XL208). The X-ray diffraction (XRD) pattern of the samples was prepared using a Quantachrome Nova2000 instrument in 2θ of 10–70°. Additionally, the elemental analysis of Fe_3O_4/AC composite was determined using a SEM equipped with energy dispersive X-ray analyzer (EDX) (Philips, XL-30). The textural properties of the samples (e.g. specific surface area and pore volume) were investigated using the Brunauer, Emmett and Teller (BET, Quantachrome, NOVA 2000) method using N_2 adsorption–desorption isotherms at 77.3 K. The magnetic properties of the composite were also evaluated by a vibrating sample magnetometer (VSM) (7400, Lakeshare, USA) at room temperature.

Batch experiments

Batch experiments were performed in a laboratory to examine the performance of Fe_3O_4/AC nanoparticles on NP removal from aqueous solution. In this regard, experiments were carried out in several 80 mL plastic bottles containing 50 mL of NP solution under different experimental variables: pH of solution (3–11), contact time (2–120 min), adsorbent dosage (0.02–1.5 g/L), and NP concentration (1–5 mg/L) at room temperature (25 ± 2 °C). The experimental bottles were placed on a shaker and then were shaken severely with the speed of 250 rpm for desired time periods. After completing the experiments, the adsorbents were extracted from the aqueous solution in an external magnetic field and the residual concentration of NP was determined using high-performance liquid chromatography (model KNAUER) equipped with an Ultimate variable wavelength UV detector (2500) set at 275 nm. Samples were injected into a 20 μL loop using a manual injector. A 100-5 C18 column (4.6 mm × 250 mm, 5 μm) was used and its temperature was set at 25 °C. The calibration curve was constructed in seven levels (in the range 0.01–10 mg/L) for NP quantification. The mobile phase consisted of 90% methanol and 10% water with a flow rate of 1 mL/min. Batch experiments were carried out with two repetitions and the average data were reported as final results. Finally, the removal efficiency ($R\%$) of

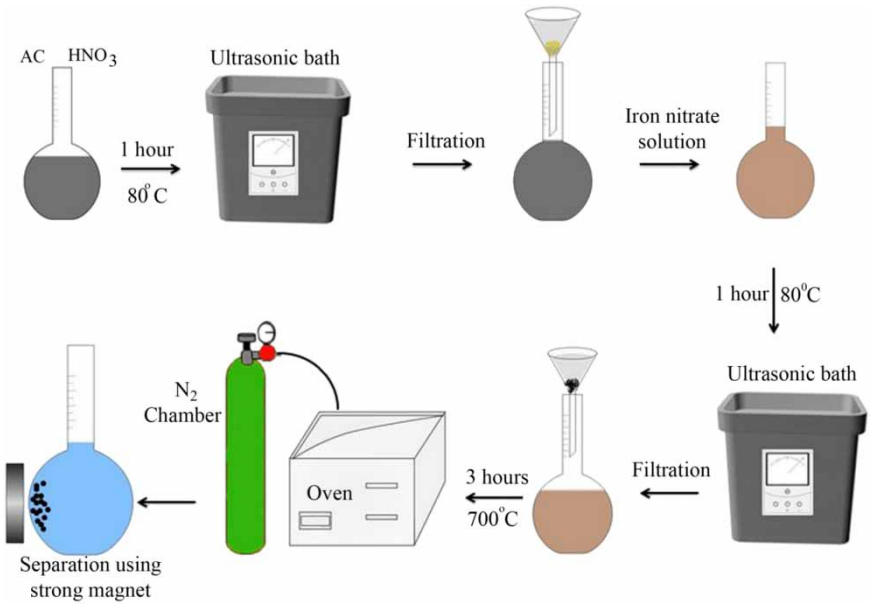

Figure 1 | Schematic picture of different steps of Fe_3O_4/AC nano-composite synthesis.

NP and the adsorption capacity (q_e) of Fe_3O_4/AC nanoparticles were calculated via the following equations:

$$R\% = 1 - \left(\frac{C}{C_0}\right) \times 100 \quad (1)$$

$$q_e = \frac{V(C_0 - C)}{m} \quad (2)$$

where V (L) is the volume of solution, and m (g) is the weight of adsorbent. Additionally, C_0 and C (mg/L) are the initial and residual adsorbate concentrations.

Adsorption kinetic and isotherm models

To design a typical adsorption system, it is critical to determine the adsorption parameters. The adsorption equilibrium is always explained by the isotherm equations, whose parameters indicate the surface characteristics and affinity of the adsorbent toward the adsorbate. In order to determine the adsorption equilibrium of NP onto the Fe_3O_4/AC composite, four isotherm models – Langmuir, Freundlich, Liu, and Temkin – were studied. For further details of these models, please see Supplementary material Table S1 (available with the online version of this paper). Additionally, the study of kinetic adsorption of NP was performed by six different models: pseudo-first-order equation of Lagergren, pseudo-second-order equation of Ho, Elovich, fractional power function, Avrami fractional order, and intra-particle diffusion. For further details of these models, please see Supplementary material Table S1.

Reusability and desorption of Fe_3O_4/AC nanoparticles

To evaluate the possibility of regeneration and reuse of the adsorbent, methanol, as a desorbing solution, was used to extract the adsorbed NP on Fe_3O_4/AC. The reusability of the adsorbents was determined using five adsorption-regeneration cycles. A sample of 0.1 g of Fe_3O_4/AC nanoparticles was shaken with 100 mL solution of 1 mg/L NP for 4 h at 25 ± 1 °C and pH 3.0. The solid product was magnetically collected, washed and then dried at 80.0 °C. Afterwards, samples of 0.05 g of Fe_3O_4/AC nanoparticles loaded with NP were shaken at 200 rpm for 24 h with 10 mL of desorbing solutions at 25 ± 1 °C. Then the desorption percentage was determined using the ratio of the weight of desorbed NP and the weight of adsorbed NP. After desorption, regenerated adsorbents were dried in an oven at 80.0 °C for 100 min and were used for the next adsorption-regeneration cycle.

RESULTS AND DISCUSSION

Characterization of Fe_3O_4/AC nanoparticles

The SEM images of AC and Fe_3O_4/AC are depicted in Figure 2(a) and 2(b), indicating that the Fe_3O_4/AC surfaces were more irregular than unmodified AC. The nanoparticles also exhibit an approximately uniform distribution of pores, with different sizes and shapes, on the surface of the activated carbon, indicating that Fe_3O_4/AC has a good porosity for the adsorption of pollutants. In addition, as can be seen, the external surface of Fe_3O_4/AC has some clump cavities, which could provide more reactive sites and a high adsorption capacity for the prepared adsorbent. The TEM micrograph of the composite shows that Fe_3O_4 particles have been successfully synthesized with an average diameter of 30–80 nm and a cubic structure (Figure 2(c)). To scrutinize the structure of the composite, the TEM image shows the granular structure of particles (Figure 2(c)). Furthermore, the elemental analysis of Fe_3O_4/AC nanoparticles is shown by the EDX spectrum (Figure 2(d)), where the sharp peaks of Fe, O and C confirm the bonding between magnetic nanoparticles and the activated carbon. Also, some minor peaks indicate the presence of Zn and Pb in the structure of the composite.

As shown in XRD analysis (Figure 2(f)), a broad diffraction peak at $2\theta = 25^\circ$ can correspond to the characteristic reflection of carbon of amorphous nature, and this peak was narrow and weaker for Fe_3O_4/AC composite when compared with the virgin AC. For Fe_3O_4 nanoparticles, the results revealed that the XRD pattern of Fe_3O_4 was in a good agreement with that of pure magnetite. As shown in Figure 2(f), six sharp peaks at 2θ values of 30.07° (220), 35.44° (311), 43.15° (400), 54.6° (422), 56.99° (511), and 62.6° (440) in the patterns of both Fe_3O_4 and Fe_3O_4/AC were attributed to the characteristic peaks of the cubic phase Fe_3O_4 according to the JCPDS No. 19-0629. These results illustrated that the Fe_3O_4 nanoparticles have successfully been coated on the AC surface.

Textural properties (specific surface area, volume and average diameter of the pores) of AC, Fe_3O_4 and Fe_3O_4/AC were analyzed using BET technique and results are presented in Table 1. The results of the BET analysis indicated that the highest surface area of adsorbent was 671.2 m^2/g, which was lower as compared to virgin AC (733 m^2/g).

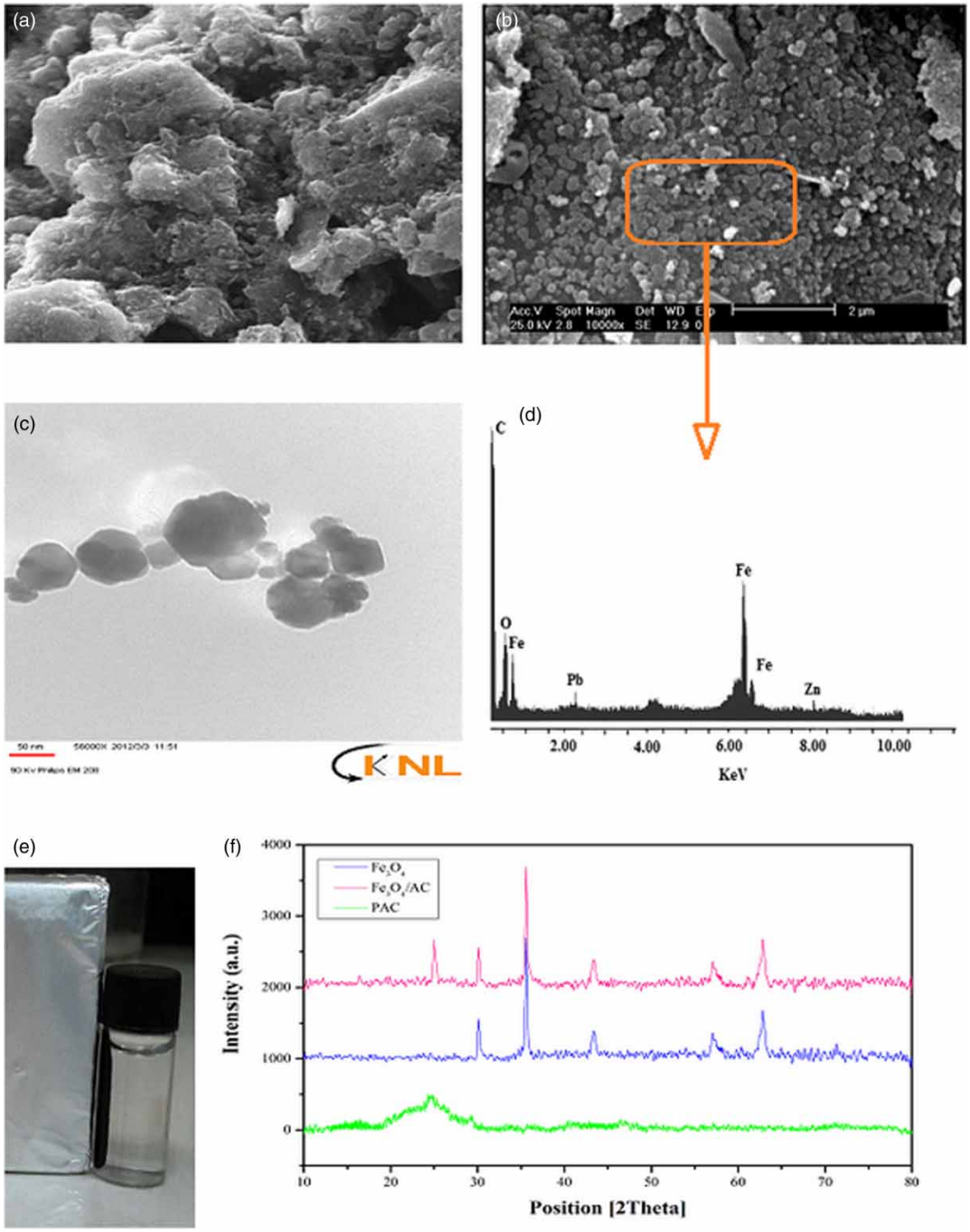

Figure 2 | (a) SEM image of AC, (b) SEM image of Fe_3O_4/AC, (c) TEM image of Fe_3O_4/AC, (d) EDX spectrum of Fe_3O_4/AC, (e) magnetic response of composite synthesis, and (f) XRD spectra of Fe_3O_4/AC.

This can be explained by the formation of Fe_3O_4 inside the AC pores and/or loss of AC pores by Fe_3O_4 nanoparticles, as reported in the literature (Kakavandi *et al.* 2016c). The average size and volume of pores of the composite were obtained to be 3.5 nm and 4.87 mL/g, respectively. This average size, based on the IUPAC classification (micropores ($d < 2$ nm), mesopores ($2 < d < 50$ nm) and macropores ($d > 50$ nm)), could be classified into the mesopores group (Jafari *et al.* 2016). Maximum saturation of magnetization (6.94 emu/g) was found to be for Fe_3O_4/AC nanoparticles according to the VSM analysis. As illustrated in Figure 2(e), the composite showed an excellent magnetic response to a

Table 1 | The microstructure and textural properties of various samples

	Sample		
Parameter	**Magnetite**	**AC**	**Fe_3O_4/AC**
Average pore diameter (nm)	4.8	3.2	3.5
Pore volume (cm^3/g)	0.006	0.76	0.48
Specific surface area (BET) (m^2/g)	62.3	733	671.2
Pore structure	Mesopore	Mesopore	Mesopore
Color	Black	Black	Black
pH_{pzc}	–	7.7	6.8

magnetic field, suggesting that it could be separated easily and rapidly due to this high magnetic sensitivity. Therefore, Fe_3O_4/AC nanoparticles can be potentially employed as a magnetic sorbent to remove pollutants from the aqueous media, avoiding a secondary pollution, without filtration and centrifuging.

Effect of experimental variables

The pH of aqueous solution is one of the most significant factors influencing the interaction between the adsorbent and the adsorbate, due to its impact on the ionization of target contaminants, surface charges of the functional groups of the adsorbents, and the degree of solubility of ions in aqueous media (Amuda *et al.* 2007). Therefore, the adsorption of NP onto the Fe_3O_4/AC was performed in the pH range of 3–11. Figure 3(a) shows that the solution pH has a fluctuating effect on the adsorption of NP by

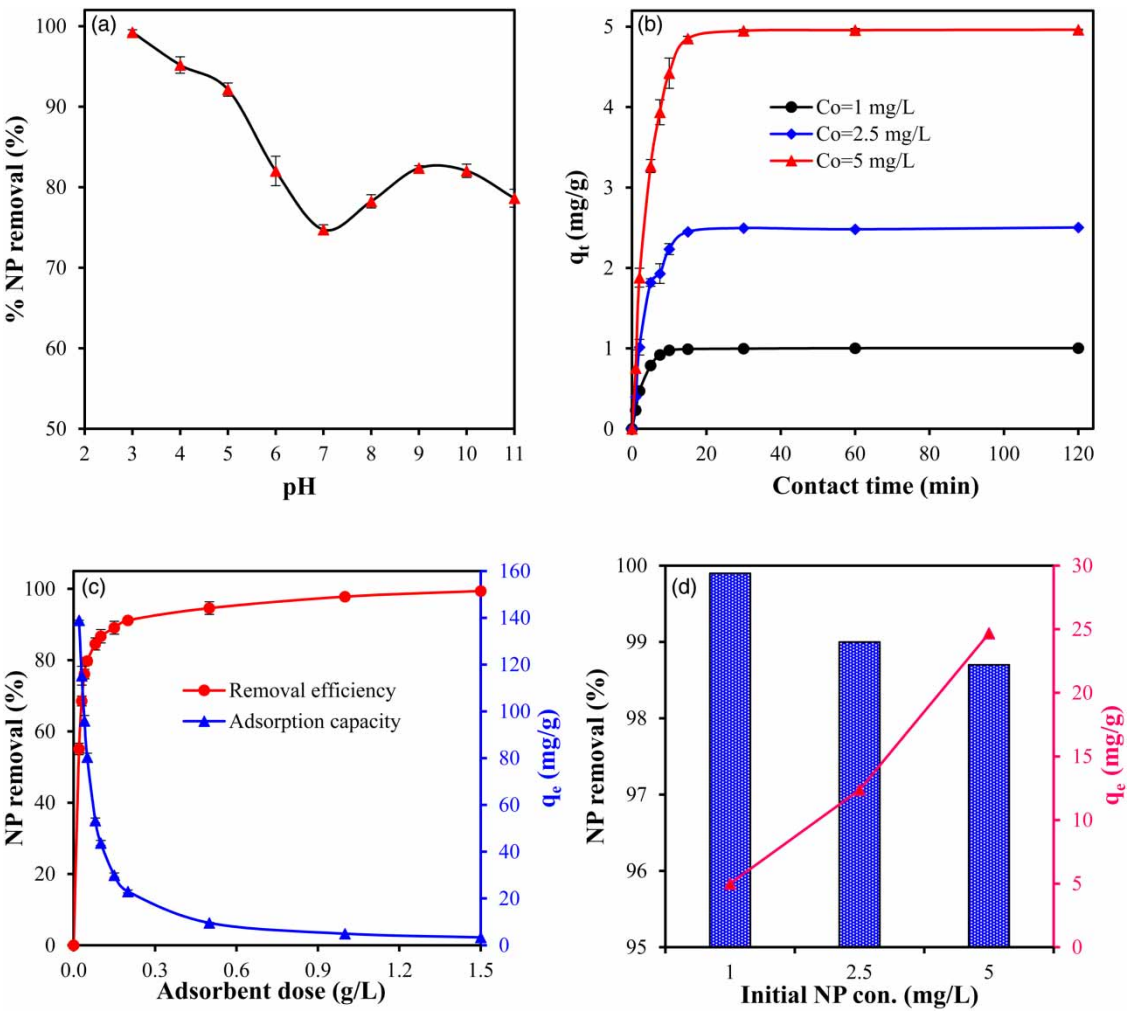

Figure 3 | (a) Effect of different pH of solution, (b) effect of contact time, (c) effect of different adsorbent dosages and (d) effect of different initial NP concentrations on NP adsorptive removal using Fe_3O_4/AC nano-composite synthesis (experimental conditions: T = 25 °C; (a) t = 120 min, adsorbent dosage = 1 g/L, C_0 = 1 mg/L; (b) pH = 3.0, adsorbent dosage = 1 g/L; (c) pH = 3.0, t = 30 min, C_0 = 5 mg/L; (d) pH = 3.0, t = 30 min, adsorbent dosage = 0.2 g/L.

means of Fe_3O_4/AC composite. The maximum NP adsorption was observed at pH of 3 (99.23%) while the graph shows a dramatic decrease to 74.72% in pH of 7. Afterwards, a sharp increase took place in NP adsorption when the NP removal increased to around 78.62% in pH of 11.

The high adsorption efficiency at pH of 3 can be attributed to the interaction between the dipole of the phenol function in NP and the positively charged Fe_3O_4/AC surfaces (Babaei *et al.* 2011). Moreover, at low pH values, which are full of hydrogen ions in solution, and hydroxyl groups form, NP did not dissociate. Under the driving of π–π stacking interaction, the hydrogen bond could be formed easily leading to an increase in the adsorption efficiency (Pan *et al.* 2013). However, at alkaline conditions, the surface of the adsorbent is negative and thus an electrostatic repulsion occurs between NP molecules for the adsorption sites, which tends to decrease the adsorption capacity. In addition, it is possible that under this condition the OH^- ions compete with NP molecules for active sites on the Fe_3O_4/AC. According to Table 1, the pH_{pzc} value of Fe_3O_4/AC was 6.8, indicating that the surface charge of the adsorbent is positive when $pH_{pzc} > pH$ and is negative at $pH_{pzc} < pH$. Therefore, at acidic conditions ($pH_{pzc} > pH$) the Fe_3O_4/AC surface charge is positive and the electrostatic force between the adsorbent surface and NP molecules increases. At pH values >6.8 ($pH_{pzc} < pH$), however, the surface charge of Fe_3O_4/AC is negative and the adsorption potential decreases significantly due to the electrostatic repulsion between NP molecules and the adsorbent surface, as illustrated in Figure 3(a).

The contact time between the adsorbate and the adsorbent is the other important parameter that affects the performance of any adsorption process. The effect of contact time on the NP adsorption capacity for initial various concentrations is illustrated in Figure 3(b). The results showed that the rate of NP adsorption onto Fe_3O_4/AC nanoparticles was rapid initially and then decreased gradually until the equilibrium was reached, beyond which there was no further adsorption. This can be explained by the fact that active sites are initially vacant and are then filled by adsorbate with increasing contact time, finally leading to a saturated adsorbent surface (Babaei *et al.* 2015). Figure 3(b) shows that the adsorption capacity of NP was almost constant for the contact times after 30 minutes at all the studied concentrations. In fact, the adsorption process reaches the equilibrium point at 30 min. Therefore, this was chosen as the equilibrium time of NP adsorption onto Fe_3O_4/AC nanoparticles.

The mass of adsorbents is another likely feature that affects the removal of any kind of contaminants. In this regard, various amounts of Fe_3O_4/AC nanoparticles as an adsorbent (0.02–1.5 g/L) were used for the adsorption of 5 mg/L NP at optimum pH of 3 which was obtained in previous experiments with 30 min contact time. Based on Figure 3(c), a direct relationship between adsorbent dosage and adsorption efficiency of NP is observed. Specifically, by increasing the adsorbent dosage from 0.02 to 0.2 g/L, adsorption efficiency of NP rose significantly from 59.93 to 98.51%. Afterwards, the graph represents a steady state pattern that confirms the optimum adsorbent dosage for NP adsorption is 0.2 g/L, which was applied in the following experiments. From these results, it can be concluded that the interaction between adsorbent and adsorbate confirms a relationship whereby sorption sites are increased by enhancing the mass of adsorbents (Farasati *et al.* 2013). This finding is in agreement with the results of previous studies reported in the literature (Babaei *et al.* 2015).

Another important experimental factor examined with regard to the adsorption of NP was the initial NP concentration. The adsorption of NP at different ion concentrations (1, 2.5 and 5 mg/L) was carried out in an optimum pH of 3 and 0.2 g/L of Fe_3O_4/AC nanoparticles for a period of 30 min at room temperature. The obtained results are illustrated in Figure 3(d). Accordingly, higher NP adsorption was observed in lower NP concentrations. In other words, increasing NP concentrations caused a significant decrease in the removal efficiency of Fe_3O_4/AC nanoparticles. As can be seen in Figure 3(d), the adsorption efficiency of NP dropped when the initial NP concentrations increased from 1 to 5 mg/L. The probable reason behind this phenomenon can be related to the filling of active sites onto the functional groups of the surfaces of adsorbents, which were intensified by increasing the initial concentrations of the adsorbate (Soltani *et al.* 2014).

Kinetic studies

The kinetic study of NP adsorption was performed by fitting the experimental data to six different kinetic models in order to find the rate constant of the adsorption process. The experimental data were fitted using non-linear regression analysis by means of MATLAB package software. Figure 4(a)–4(c) represent the kinetic plots of NP adsorption at different initial concentrations based on the contact time (t) against NP adsorption capacity (q). The obtained parameters and constants of applied models are reported

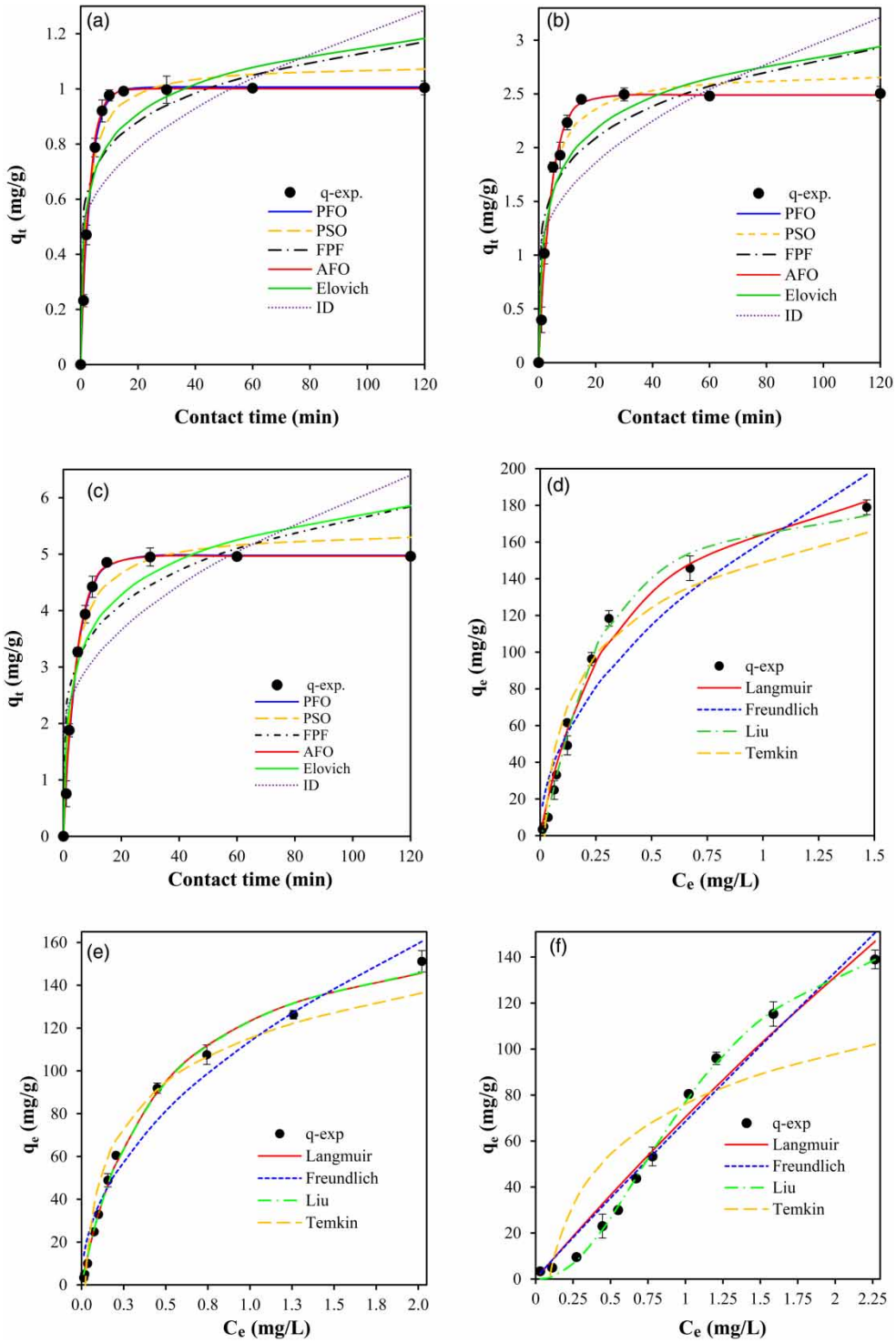

Figure 4 | Kinetic (a)–(c) and isotherm (d)–(f) adsorption graphs of NP adsorption onto Fe_3O_4/AC composite (experimental conditions: pH = 3.0, T = 25 °C; (a)–(c) adsorbent dose = 0.2 g/L, C_0 = 1–5 mg/L; (d)–(f) t = 30 min, C_0 = 5 mg/L, adsorbent dosage = 0.02–1.5 g/L, T = 10–40 °C).

in Table 2. According to this table, among all kinetic models, pseudo-first-order and Avrami could better fit the experimental data of NP adsorption with a significant high coefficient of correlation (R^2) (>0.99) in all the studied concentrations. In addition, it is strongly suggested in Table 2 that the calculated equilibrium adsorption capacity, $q_{e,\ cal}$,

Table 2 | Kinetic parameters for NP adsorption onto Fe_3O_4/AC nano-composite at different temperatures

Adsorption kinetic models	Parameters	Initial NP conc. (mg/L)		
		1.0 mg/L	2.5 mg/L	5.0 mg/L
Pseudo-first-order	q_e (mg/g)	1	2.5	4.9
	k_f (min^{-1})	0.30	0.23	0.22
	R^2	0.998	0.99	0.997
	R^2adj	0.998	0.993	0.997
	SSE	0.002	0.05	0.07
	RMSE	0.015	0.08	0.09
Pseudo-second-order	k_S (g/mg·min)	0.41	0.12	0.05
	q_e (mg/g)	1.1	2.7	5.4
	R^2	0.97	0.976	0.977
	R^2adj	0.967	0.973	0.974
	SSE	0.037	0.19	0.73
	RMSE	0.067	0.15	0.3
Fractional power function	a	0.55	1.2	2.3
	b	0.16	0.19	0.192
	R^2	0.8	0.8	0.81
	R^2adj	0.77	0.79	0.791
	SSE	0.24	1.4	5.87
	RMSE	0.17	0.42	0.85
Avrami fractional order	k_{AV} (min^{-1})	0.3	0.234	0.22
	q_e (mg/g)	1.	2.5	4.9
	n_{AV}	1.08	0.998	1.03
	R^2	0.999	0.993	0.998
	R^2adj	0.999	0.992	0.997
	SSE	0.0009	0.05	0.067
	RMSE	0.0114	0.085	0.098
Elovich	α (mg/g·min)	2.97	3.44	5.73
	β (g/mg)	6.5	2.34	1.14
	R^2	0.857	0.881	0.883
	R^2adj	0.84	0.866	0.868
	SSE	0.177	0.936	3.7
	RMSE	0.148	0.342	0.68
Intra-particle diffusion	k_{id} (mg/g·$min^{1/2}$)	0.07	0.21	0.42
	C	0.44	0.927	1.76
	R^2	0.489	0.563	0.576
	R^2adj	0.425	0.51	0.523
	SSE	0.632	3.43	13.4
	RMSE	0.281	0.655	1.3

using pseudo-first-order and Avrami models, is very close to the experimental $q_{e,\ exp}$ values. This means that the adsorption process fitted better to these models.

As shown in Table 2, the values of rate constants (k_f, k_s and k_{Av}) decrease by increasing the initial NP concentration. This can be due to the high competition of adsorbate molecules for the adsorption surface sites at high concentrations, which leads to lower sorption rates. This observation has also been reported by other researchers studying the adsorption of contaminants (Depci *et al.* 2012; Azari *et al.* 2015).

The intra-particle diffusion model can be used to verify the influence of mass transfer resistance on the binding of adsorbate to the adsorbent. NP is probably transported from aqueous solution to the adsorbents by intra-particle diffusion. To investigate this issue, the results for kinetic adsorption were fitted with the intra-particle diffusion model. The lower values of R^2 for the intra-particle diffusion model show that this model is not applicable for NP adsorption on Fe_3O_4/AC nanoparticles. Furthermore, as observed in Table 2, the values of C of the intra-particle diffusion model are not equal to zero at any of the studied concentrations, indicating that intra-particle diffusion is not the only controlling step for the NP adsorption process. Hence, other mechanisms such as complexes or ion-exchange may also control the rate of adsorption (Kakavandi *et al.* 2016a).

Isotherm studies

Isotherm investigation is one of the most integral types of adsorption studies that evaluate the reaction between both the adsorbate and the adsorbent. Therefore, we studied the isotherm behavior of NP adsorption onto the surfaces of Fe_3O_4/AC composite using four models. Like the kinetic studies, isotherm parameters were fitted via non-linear regression analysis using the MATLAB software package. The non-linear graphs of the isotherm of NP adsorption at different temperatures, drawn based on q_e vs. C_e, are given in Figure 4(d)–4(f). Additionally, Table 3 shows the obtained isotherm parameters of NP adsorption. According to Table 3, of all the applied models, Liu was more capable of fitting adsorption data of NP removal with its high coefficient of determination ($R^2 > 0.99$) and the low root-mean-squared error (RMSE) and sum of squared error (SSE) values in all temperatures. On the other hand, in the same experimental conditions, Temkin was found to be the least suitable isotherm model in fitting NP adsorption data. Also, the adsorption capacities of the Liu model represent a direct relationship with temperature: adsorption capacity decreased significantly by increasing temperature, illustrating that the process of NP adsorption is exothermic in nature. The Liu isotherm model is intrinsically a mixture of both the Freundlich and Langmuir models; therefore, the monolayer hypothesis of the Langmuir model is eliminated and the infinite adsorption assumption specifically rooted from the Freundlich model is also overruled. This model predicts that all the reactive sites on the surfaces of the adsorbent have no similar energy. Hence, the adsorbent may have active sites preferred by the adsorbate molecules

Table 3 | Isotherm parameters for NP adsorption onto Fe_3O_4/AC nano-composite at different temperatures

Adsorption isotherm models	Parameters	Temperature 283 K	298 K	313 K
Langmuir	q_m (mg/g)	226.5	177.3	1,033
	b (L/mg)	2.8	2.29	0.073
	R^2	0.984	0.995	0.968
	R^2adj	0.982	0.995	0.965
	SSE	582.6	3.65	694.6
	RMSE	8.04	119.8	8.78
Freundlich	K_F (L/g)	162.3	113.8	68.5
	n	1.98	2.05	1.04
	R^2	0.922	0.966	0.965
	R^2adj	0.913	0.962	0.961
	SSE	2,855	10.1	778.2
	RMSE	17.81	912.9	9.3
Redlich–Peterson	K_{RP} (L/g)	532.3	448.7	71.3
	a_{RP} (L/mg)	2.14	2.68	1.738E − 08
	g (−)	1.24	0.924	19.6
	R^2	0.988	0.996	0.979
	R^2adj	0.986	0.995	0.974
	SSE	410.5	3.58	455.9
	RMSE	7.16	103	7.55
Liu	K_g (L/mg)	4.44	2.23	0.936
	n	1.4	0.9873	2.181
	q_m (mg/g)	187.2	179.1	165.8
	R^2	0.994	0.995	0.998
	R^2adj	0.993	0.994	0.997
	SSE	206.5	3.86	45.8
	RMSE	5.1	119.4	2.39
Temkin	A (L/g)	52.02	46.7	11.03
	B	38.12	30	31.7
	R^2	0.92	0.953	0.713
	R^2adj	0.91	0.948	0.68
	SSE	2,958	11.8	6,330
	RMSE	18.1	1,250	26.5

for occupation. However, saturation of the active sites should occur in contrast to what occurs in the Freundlich isotherm model. Considering various functional groups on the Fe_3O_4/AC nanoparticles, our results show that the active sites of the Fe_3O_4/AC will not naturally be able to share the same amounts of energy. Based on the Liu model assumptions, all reactive sites on the surface of the adsorbent have no similar energy. Hence, the adsorbent would have several reactive sites that tend to be occupied with the adsorbate molecules (Jafari *et al.* 2016).

As seen in Table 3, the values of n of the Freundlich model in the range of 1–10 is an appropriate index to prove the reliability of the adsorbent. Based on Table 3, n varies from 1.04 to 2.04 in all temperatures, showing the applied composite is a promising adsorbent for NP removal. The K_F of Freundlich also decreased from 162.3 to 68.56 L/g, which indicates that the adsorption process of NP is exothermic (Yang *et al.* 2011).

Thermodynamic studies

Temperature is an essential parameter that governs the adsorption process. The thermodynamic studies were performed at different temperatures (283, 298 and 313 K) in order to calculate the thermodynamic parameters of NP adsorption. The thermodynamic parameters of Arrhenius activation energy (Ea) and change in free energy (ΔG^o), enthalpy (ΔH^o), and entropy (ΔS^o) of the adsorption process were calculated according to Equations (3)–(5)) (Kakavandi *et al.* 2016a). More details of these parameters are given in the Supplementary material (available with the online version of this paper).

$$\ln k_{AV} = \ln k_{\circ} - \frac{Ea}{RT} \tag{3}$$

$$\Delta G^o = -RT \ln K \tag{4}$$

$$\ln K = \frac{\Delta S^o}{R} - \frac{\Delta H^o}{RT} \tag{5}$$

The magnitude of activation energy gives information about the type of adsorption. The physisorption process usually has energies in the range of 5–40 kJ/mol, while higher activation energies (40–800 kJ/mol) suggest chemisorption (Babaei *et al.* 2015). The activation energy was calculated to be 6.8 kJ/mol, indicating that the adsorption of NP onto the Fe_3O_4/AC was a physisorption process (Jafari *et al.* 2016).

According to the thermodynamic results, the obtained ΔG^o was negative in all temperatures indicating the spontaneous nature of the adsorption process (see Table 4). The negative value of ΔH^o (−38.1 KJ/mol) also showed that the process of NP adsorption onto Fe_3O_4/AC is exothermic. Enthalpy change value between 2.1 and 20.9 kJ/mol is frequently considered to indicate physical

Table 4 | The values of thermodynamic parameters of NP adsorption on Fe_3O_4/AC composite

T (K)	ΔH° (kJ/mol)	ΔS° (J/mol)	ΔG° (kJ/mol)
283	−38.1	−7.1	−36.0
298			−36.1
313			−35.9

adsorption processes, whereas for chemical adsorption it lies in the range of 80–200 kJ/mol. In this work, the ΔH° value was found to be −38.1 kJ/mol, suggesting that the transportation of NP ions from the aqueous solution to the Fe_3O_4/AC composite surface occurred physically, which is consistent with the results obtained from the activation energy of the adsorption (Babaei *et al.* 2015). Additionally, from the negative value of ΔS^{o}, it can be postulated that a drop occurs in the randomness of the solid/surface interface at the internal structure of the NP adsorption onto the applied composite.

ANN studies

ANNs are useful simulation methods directly inspired from the biology of the human brain, where a variety of complex information is processed by billions of neurons (Salari *et al.* 2009). ANN topology consists of layers, neurons (nodes) in each layer, and the nature of transfer functions. Each ANN unit includes an input layer, hidden layers, and an output layer. The input layer consists of nodes related to input variables (Kıranşan *et al.* 2015). In this study, the input variables represent operational parameters including the solution pH, the contact time (min), the initial NP concentrations (mg/L), and the adsorbent dosage (g/L). The hidden layers of the model enable the model to evaluate the complex interactions between input and output data. The output layer has a node which corresponds to the output variable (experimental response). The schematic diagram of the applied model is illustrated in Figure 5(a). The applied training function in this study was a linear transfer one and the training-and-test method was used to evaluate the ANN. All input and output data in ANN must have been scaled within a specified range. Accordingly, all

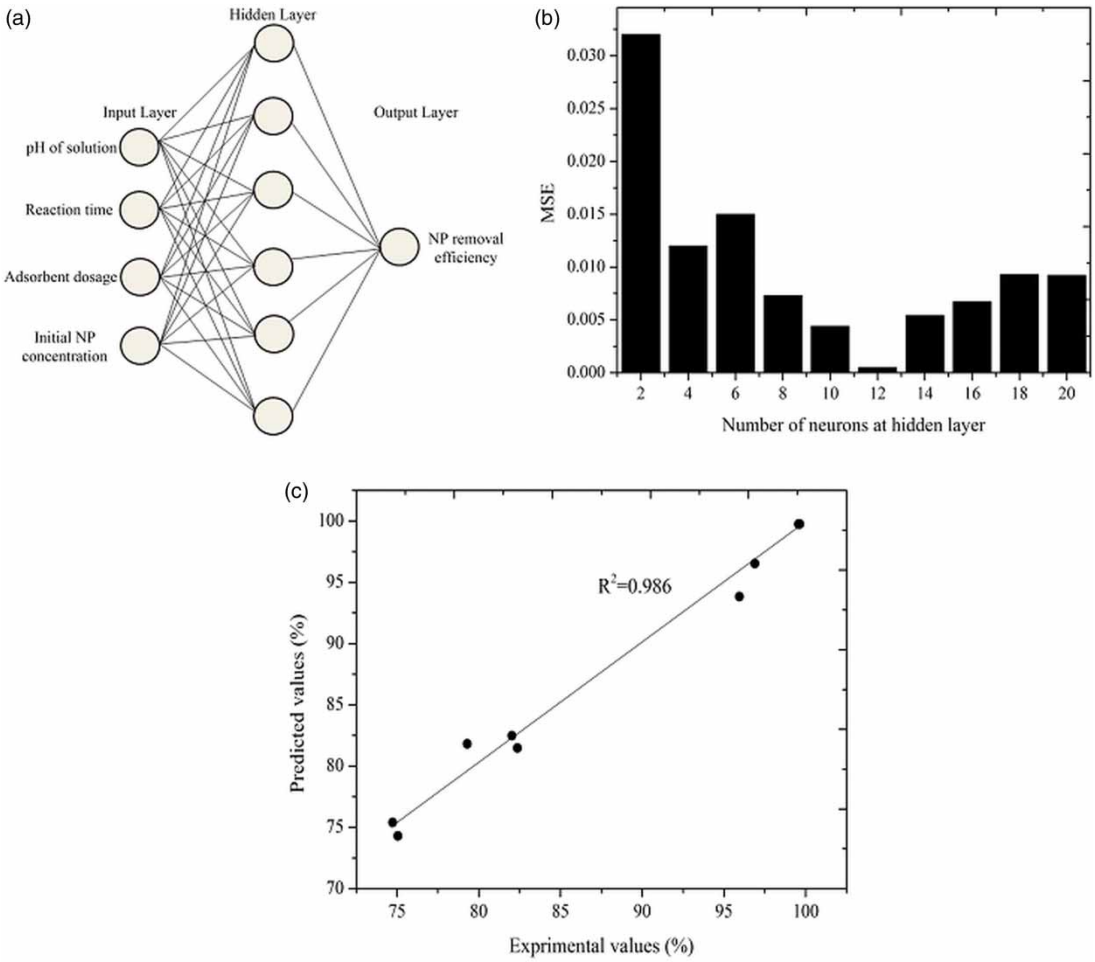

Figure 5 | (a) The schematic graph of applied ANN in this study, (b) the agreement between the predicted ANN model and the experimental values of NP removal efficiency and (c) scatter plot of experimental values of NP adsorption versus ANN predicted ones.

obtained experimental values (X_i) were scaled into the 0.1–0.9 range values (x_i) as follows:

$$x_i = \frac{0.8(X_i - X_{\min})}{(X_{\max} - X_{\min})} + 0.1 \quad (6)$$

where $X_{\min}$ and $X_{\max}$ are minimum and maximum actual experimental values of data sets, respectively (Kıranşan *et al.* 2015).

During the training phase, each node received the input signals from input data or nodes of previous lines and biases, aggregated them by using the weights, and passed the result after suitable transformation as the output signal through a transfer function. Then the weights were adjusted by back-propagating the error calculated from the difference between the predicted and the experimental outputs (Esfahani *et al.* 2014b).

To find the optimal number of nodes in the hidden layer and the best possible weights and biases, the numbers of nodes were varied from 2 to 20. The optimum number of hidden nodes was determined by using mean square error (MSE) of the training and validation sets. According to the obtained results (Figure 5(b)), MSE decreased as the number of neurons was increased up to 12 and then increased. Therefore, input, hidden and output layers, respectively, with 4, 12 and 1 neurons were selected as the optimum ANN topography. The set of connection weights and biases that cause the optimum ANN topography are listed in Table 5.

Validity of the formulated ANN model was tested by comparing the model-predicted values of MB adsorption onto the Fe_3O_4/AC nanoparticles with those experimentally obtained (Figure 5(c)). Accordingly, the high correlation coefficient ($R^2 = 0.986$) proves the reliability of ANN to predict the adsorptive removal of MB.

Equation (7) was used to make a quantitative estimate of the relative importance (I_j) of pH, the contact time, the initial NP concentrations and the adsorbent dosage on MB adsorption according to the weights produced by the ANN model:

$$I_j = \frac{\sum_{m=1}^{m-N_h}\left(\left|W_{jm}^{ih}\right| / \sum_{k=1}^{N_i}\left|W_{km}^{ih}\right|\right) \times \left|W_{mn}^{ho}\right|}{\sum_{k=1}^{k=N_i}\left\{\sum_{m=1}^{m=N_h}\left(\left|W_{km}^{ih}\right| / \sum_{k=1}^{N_i}\left|W_{km}^{ih}\right|\right) \times \left|W_{mn}^{ho}\right|\right\}} \quad (7)$$

where N_i and N_h are the number of the nodes in inputs and hidden layers, respectively. W is the connection weight in which the superscripts 'i', 'h', and 'o' are attributed to input, hidden, and output layers, respectively; and subscripts 'k', 'm', and 'n' are attributed to input, hidden, and output nodes, respectively.

The relative importance of each variable on the adsorption efficiency of NP has been reported in Table 6. All of the investigated variables strongly influence the NP adsorption onto the Fe_3O_4/AC composite and cannot be neglected, but the pH of aqueous solution plays the most pivotal role on the adsorption process.

Table 5 | Matrices of ANN optimized structure weights

Weights and biases between input and hidden layers

	Variable				
Neuron of hidden layer	pH	Reaction time (min)	Initial NP concentration (mg/L)	Adsorbent dosage (g/L)	Bias
1	0.456	0.172	0.0113	0.167	2.66
2	0.272	0.047	0.885	0.253	2.29
3	0.08	0.04	0.105	0.073	2.68
4	0.24	0.16	0.23	0.25	2.1
5	1.65	0.26	0.74	0.56	1.38
6	0.198	0.15	0.23	0.19	0.7
7	0.02	0.02	0.016	0.002	0.43
8	0.14	0.21	0.4	0.17	0.65
9	2.2	0.63	0.66	1.04	3.38
10	0.2	0.59	0.68	0.41	1.77
11	0.71	0.019	1.03	0.78	2.77
12	0.29	2.63	0.45	0.62	3.81

Weights and bias between hidden and output layers

Neuron of hidden layer	Weights	Bias
1	0.8	0.29
2	1.46	
3	0.29	
4	0.88	
5	3.2	
6	0.77	
7	0.06	
8	0.93	
9	4.54	
10	1.49	
11	2.55	
12	3.99	

Recycling and regeneration of Fe_3O_4/AC nanoparticles

The regeneration of adsorbent and the restoration of adsorption capability is a crucial factor in the practical application

Table 6 | Experimental variable ranges and their impacts on NP adsorption efficiency

Experimental variable	Range	Significance (%)
pH of solution	3–11	30
Reaction time (min)	1–30	23
Adsorbent dosage (g/L)	0.02–1.5	21
Initial NP concentration (mg/L)	1–5	26

of the adsorbent. The results from adsorption–desorption experiments are presented in Figure 6(a). It shows that the adsorption percentage of NP by Fe_3O_4/AC nanoparticles decreased insignificantly from 99.6 to 92.6% after the fifth cycle. This proves that the synthesized composite can be recycled and reused for at least five successive cycles with an adsorption efficiency >90%. It was also observed that the desorption efficiencies did not change noticeably by increasing desorption cycles. As seen in Figure 6(a), more than 92.0% of the adsorbed NP could be desorbed and recovered from the Fe_3O_4/AC nanoparticles surface in the presence of methanol in the fifth cycle. These results suggest that the Fe_3O_4/AC nanoparticles have a good potential for regeneration and reusability. Therefore, they can serve as an economical and effective adsorbent for NP removal from aqueous solutions in industrial applications based on simple and easy regeneration with acid treatment for NP adsorption.

Treatment of a simulated NP-house effluent

In order to investigate the removal potential of NP using the Fe_3O_4/AC nanoparticles in real environments, the adsorption performance was evaluated in three samples, river water, tap water and wastewater effluent, under the optimized conditions. The percentage of NP adsorption by the Fe_3O_4/AC in the above samples containing 1 mg/L concentrations of NP are shown in Figure 6(b). Under these conditions, the adsorption efficiencies of 70.7, 73.5 and 67.3% were observed for the river water, the tap water and the wastewater effluent, respectively. According to Figure 6(b), there was no significant difference in the removal percentages of NP using Fe_3O_4/AC nanoparticles for the investigated samples. This means that other substances which are present in the river water or wastewater effluent do not have a noticeable influence on the adsorption percentage of NP onto the Fe_3O_4/AC nanoparticles. These results illustrate that Fe_3O_4/AC nanoparticles have a good potential for the removal of NP in real samples. Therefore, the removal of NP from full scale using Fe_3O_4/AC nanoparticles as a suitable adsorbent can be a cost–effective and useful technique.

CONCLUSION

Batch experiments were carried out to evaluate the performance of Fe_3O_4/AC grafted iron oxide nanoparticles on adsorptive removal of NP from solutions. Findings revealed fast NP removal at pH of 3 and 30 min contact time. A sharp increase in NP adsorption efficiency was observed by enhancing adsorbent dosage, whereas decreasing initial NP concentrations increased NP adsorption efficiency. In addition, the adsorption process of NP removal followed

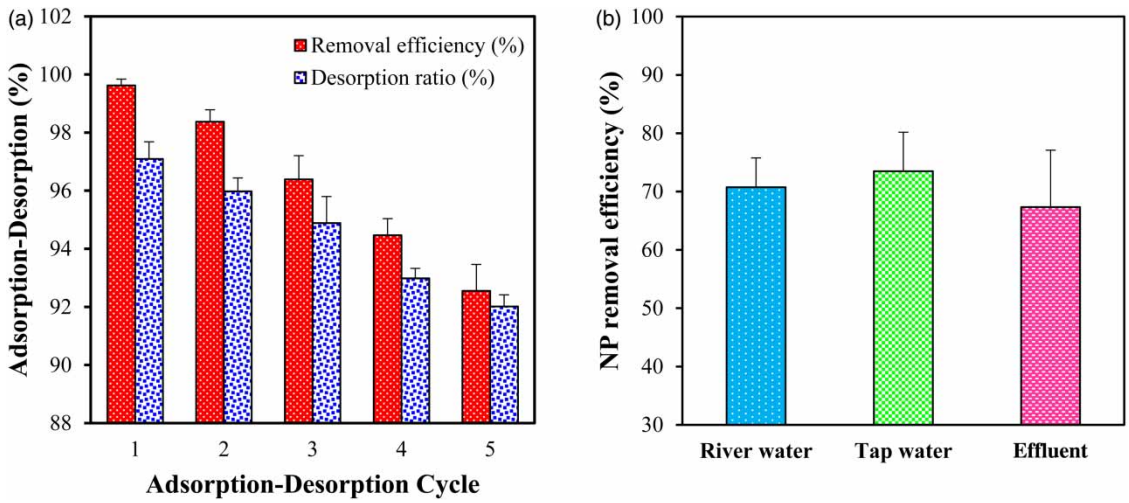

Figure 6 | (a) Five cycles of NP adsorption–desorption and (b) the comparison of the adsorption NP percentage using Fe_3O_4/AC composite in the various aquatic environments (experimental conditions: pH = 3.0, t = 30 min, adsorbent dosage = 0.2 g/L, C_0 = 1 g/L and T = 40 °C).

the Liu isotherm model and Avrami fractional order kinetic model. The negative values of thermodynamic parameters (i.e., ΔG^o and ΔH^o) showed that the contact of Fe_3O_4/AC nanoparticles with NP is spontaneous and exothermic. Furthermore, according to the results of ANN studies, pH of solution was the most effective input variable affecting NP adsorption efficiency, and initial NP concentration, contact time and adsorbent dosage were placed at the next steps, respectively. All in all, it can be found from this research that the as-synthesized composite is an efficient adsorbent that not only can remediate aqueous media from NP but also could be separated easily by means of a magnetic field.

ACKNOWLEDGEMENTS

The authors of this research gratefully acknowledge Ahvaz Jundishapur University of Medical Sciences for its academic and financial supports.

REFERENCES

Amuda, O., Giwa, A. & Bello, I. 2007 Removal of heavy metal from industrial wastewater using modified activated coconut shell carbon. *Biochemical Engineering Journal* **36** (2), 174–181.

Armenante, P. M., Kafkewitz, D., Lewandowski, G. A. & Jou, C.-J. 1999 Anaerobic–aerobic treatment of halogenated phenolic compounds. *Water Research* **33** (3), 681–692.

Asgari, G., Ramavandi, B., Rasuli, L. & Ahmadi, M. 2013 Cr (VI) adsorption from aqueous solution using a surfactant-modified Iranian zeolite: characterization, optimization, and kinetic approach. *Desalination and Water Treatment* **51** (31–33), 6009–6020.

Azari, A., Kalantary, R. R., Ghanizadeh, G., Kakavandi, B., Farzadkia, M. & Ahmadi, E. 2015 Iron–silver oxide nanoadsorbent synthesized by co-precipitation process for fluoride removal from aqueous solution and its adsorption mechanism. *RSC Advances* **5** (106), 87377–87391.

Babaei, A. A., Mesdaghiniai, A. R., Haghighi, N. J., Nabizadeh, R. & Mahvi, A. H. 2011 Modeling of nonylphenol degradation by photo-nanocatalytic process via multivariate approach. *Journal of Hazardous Materials* **185** (2–3), 1273–1279.

Babaei, A. A., Khataee, A., Ahmadpour, E., Sheydaei, M., Kakavandi, B. & Alaee, Z. 2015 Optimization of cationic dye adsorption on activated spent tea: equilibrium, kinetics, thermodynamic and artificial neural network modeling. *Korean Journal of Chemical Engineering* **33** (4), 1352–1361.

Balci, B., Keskinkan, O. & Avci, M. 2011 Use of BDST and an ANN model for prediction of dye adsorption efficiency of *Eucalyptus camaldulensis* barks in fixed-bed system. *Expert Systems with Applications* **38** (1), 949–956.

Bester, K., Theobald, N. & Schröder, H. F. 2001 Nonylphenols, nonylphenol-ethoxylates, linear alkylbenzenesulfonates (LAS) and bis (4-chlorophenyl)-sulfone in the German Bight of the North Sea. *Chemosphere* **45** (6), 817–826.

Birkett, J. W. & Lester, J. N. 2002 *Endocrine Disrupters in Wastewater and Sludge Treatment Processes.* Lewis Publishers, Boca Raton, FL, USA.

Depci, T., Kul, A. R. & Önal, Y. 2012 Competitive adsorption of lead and zinc from aqueous solution on activated carbon prepared from Van apple pulp: study in single-and multi-solute systems. *Chemical Engineering Journal* **200**, 224–236.

Esfahani, A. R., Firouzi, A. F., Sayyad, G. & Kiasat, A. 2014a Transport and retention of polymer-stabilized zero-valent iron nanoparticles in saturated porous media: effects of initial particle concentration and ionic strength. *Journal of Industrial and Engineering Chemistry* **20** (5), 2671–2679.

Esfahani, A. R., Hojati, S., Azimi, A., Farzadian, M. & Khataee, A. 2014b Enhanced hexavalent chromium removal from aqueous solution using a sepiolite-stabilized zero-valent iron nanocomposite: impact of operational parameters and artificial neural network modeling. *Journal of the Taiwan Institute of Chemical Engineers* **49**, 172–182.

Farasati, M., Seyedian, M., Boroomandnasab, S., Jaafarzadeh, N., Moazed, H. & Ghamarnia, H. 2013 Batch and column studies on the evaluation of micrometer and nanometer *Phragmites australis* for nitrate removal. *Desalination and Water Treatment* **51** (28–30), 5863–5872.

Fonseca, S. M., Barker, A. L., Ahmed, S., Kemp, T. J. & Unwin, P. 2004 Scanning electrochemical microscopy investigation of the photodegradation kinetics of 4-chlorophenol sensitised by TiO_2 films. *Physical Chemistry Chemical Physics* **6** (22), 5218–5224.

Hassani, A., Vafaei, F., Karaca, S. & Khataee, A. 2014 Adsorption of a cationic dye from aqueous solution using Turkish lignite: kinetic, isotherm, thermodynamic studies and neural network modeling. *Journal of Industrial and Engineering Chemistry* **20** (4), 2615–2624.

Ide, Y., Koike, Y. & Ogawa, M. 2011 Molecular selective photocatalysis by TiO_2/nanoporous silica core/shell particulates. *Journal of Colloid and Interface Science* **358** (1), 245–251.

Jafari, A. J., Kakavandi, B., Kalantary, R. R., Gharibi, H., Asadi, A., Azari, A., Babaei, A. A. & Takdastan, A. 2016 Application of mesoporous magnetic carbon composite for reactive dyes removal: process optimization using response surface methodology. *Korean Journal of Chemical Engineering* **33** (10), 2878–2890.

Kakavandi, B., Kalantary, R. R., Jafari, A. J., Nasseri, S., Ameri, A., Esrafili, A. & Azari, A. 2015 Pb(II) adsorption onto a magnetic composite of activated carbon and superparamagnetic Fe_3O_4 nanoparticles: experimental and modeling study. *CLEAN – Soil, Air, Water* **43** (8), 1157–1166.

Kakavandi, B., Jahangiri-rad, M., Rafiee, M., Esfahani, A. R. & Babaei, A. A. 2016a Development of response surface methodology for optimization of phenol and p-chlorophenol adsorption on magnetic recoverable carbon. *Microporous and Mesoporous Materials* **231**, 192–206.

Kakavandi, B., Jonidi Jafari, A., Rezaei Kalantary, R., Nasseri, S., Esrafili, A., Gholizadeh, A. & Azari, A. 2016b Simultaneous adsorption of lead and aniline onto magnetically recoverable carbon: optimization, modeling and mechanism. *Journal of Chemical Technology & Biotechnology* **91**, 3000–3010.

Kakavandi, B., Takdastan, A., Jaafarzadeh, N., Azizi, M., Mirzaei, A. & Azari, A. 2016c Application of Fe_3O_4@C catalyzing heterogeneous UV-Fenton system for tetracycline removal with a focus on optimization by a response surface method. *Journal of Photochemistry and Photobiology A: Chemistry* **314**, 178–188.

Khataee, A., Fathinia, M., Aber, S. & Zarei, M. 2010 Optimization of photocatalytic treatment of dye solution on supported TiO_2 nanoparticles by central composite design: intermediates identification. *Journal of Hazardous Materials* **181** (1), 886–897.

Kıranşan, M., Khataee, A., Karaca, S. & Sheydaei, M. 2015 Artificial neural network modeling of photocatalytic removal of a disperse dye using synthesized of ZnO nanoparticles on montmorillonite. *Spectrochimica Acta Part A: Molecular and Biomolecular Spectroscopy* **140**, 465–473.

Kuramitz, H., Saitoh, J., Hattori, T. & Tanaka, S. 2002 Electrochemical removal of p-nonylphenol from dilute solutions using a carbon fiber anode. *Water Research* **36** (13), 3323–3329.

Liping, L., Guanghuan, C., Jingyou, D., Mingyang, S., Huanyu, C., Qiang, Y. & Xinhua, X. 2014 Mechanism of and relation between the sorption and desorption of nonylphenol on black carbon-inclusive sediment. *Environmental Pollution* **190**, 101–108.

Liu, T., Yang, Y., Wang, Z.-L. & Sun, Y. 2015 Remediation of arsenic (III) from aqueous solutions using improved nanoscale zero-valent iron on pumice. *Chemical Engineering Journal* **288**, 739–744.

Mohseni-Bandpi, A., Kakavandi, B., Kalantary, R. R., Azari, A. & Keramati, A. 2015 Development of a novel magnetite-chitosan composite for the removal of fluoride from drinking water: adsorption modeling and optimization. *RSC Advances* **5** (89), 73279–73289.

Öman, C. & Hynning, P.-Å. 1993 Identification of organic compounds in municipal landfill leachates. *Environmental Pollution* **80** (3), 265–271.

Pan, J., Li, L., Hang, H., Ou, H., Zhang, L., Yan, Y. & Shi, W. 2013 Study on the nonylphenol removal from aqueous solution using magnetic molecularly imprinted polymers based on fly-ash-cenospheres. *Chemical Engineering Journal* **223**, 824–832.

Petrovic, M., Barceló, D., Diaz, A. & Ventura, F. 2003 Low nanogram per liter determination of halogenated nonylphenols, nonylphenol carboxylates, and their non-halogenated precursors in water and sludge by liquid chromatography electrospray tandem mass spectrometry. *Journal of the American Society for Mass Spectrometry* **14** (5), 516–527.

Salari, D., Niaei, A., Khataee, A. & Zarei, M. 2009 Electrochemical treatment of dye solution containing CI Basic Yellow 2 by the peroxi-coagulation method and modeling of experimental results by artificial neural networks. *Journal of Electroanalytical Chemistry* **629** (1), 117–125.

Shirmardi, M., Mahvi, A. H., Hashemzadeh, B., Naeimabadi, A., Hassani, G. & Niri, M. V. 2013 The adsorption of malachite green (MG) as a cationic dye onto functionalized multi walled carbon nanotubes. *Korean Journal of Chemical Engineering* **30** (8), 1603–1608.

Soltani, R., Khorramabadi, G. S., Khataee, A. & Jorfi, S. 2014 Silica nanopowders/alginate composite for adsorption of lead (II) ions in aqueous solutions. *Journal of the Taiwan Institute of Chemical Engineers* **45** (3), 973–980.

USEPA (United States Environmental Protection Agency) 1996 *Analysis of the Impacts of Control Programs on Motor Vehicle Toxic Emissions and Exposure Nationwide*. Volume I. US Environmental Protection Agency, Office of Transportation and Air Quality.

Xing, M., Xu, L. & Wang, J. 2016 Mechanism of Co (II) adsorption by zero valent iron/graphene nanocomposite. *Journal of Hazardous Materials* **301**, 286–296.

Yang, G. P., Ding, H. Y., Cao, X. Y. & Ding, Q. Y. 2011 Sorption behavior of nonylphenol on marine sediments: effect of temperature, medium, sediment organic carbon and surfactant. *Marine Pollution Bulletin* **62**, 2362–2369.

First received 28 July 2016; accepted in revised form 31 October 2016. Available online 15 November 2016